Electr Eng (2007) 90:95–106
DOI 10.1007/s00202-006-0057-8

ORIGINAL PAPER

Disturbance-observer-based adaptive feedforward cancellation of torque ripples in harmonic drive systems

Yu-Sheng Lu · Shuan-Min Lin

Received: 30 August 2006 / Accepted: 15 December 2006 / Published online: 13 February 2007

Abstract This paper proposes a scheme for controlling the output torque of a harmonic drive actuator equipped with a torque sensor. The control scheme consists of the internal model control (IMC) and an adaptive feedforward cancellation (AFC) based on a disturbance observer (DOB). The relationship between the IMC and the DOB is presented in this paper, and the IMC is adopted as a feedback compensator for its ease in design and implementation. The DOB, on the other hand, is suitable for estimating an unknown disturbance, and its output is applied to the AFC resonator that generates an adaptive dither to compensate for the torque ripples induced by harmonic drives. Compared with the conventional AFC, the salient features of the proposed DOB-based AFC include the independence of designing the AFC's adaptation gain from the plant and the feedback compensator, fast convergence of the disturbance-cancellation error, and no influence of aperiodic reference changes upon the adaptive dither. The effectiveness of the proposed scheme is demonstrated through experimental results, in which its performance is shown to be superior to that of the conventional AFC.

Keywords Harmonic drive actuator · Torque control · Torque ripple · Adaptive feedforward cancellation · Disturbance observer · Internal model control

Y.-S. Lu (✉) · S.-M. Lin
National Yunlin University of Science and Technology,
123, Section 3, University Road, Touliu,
Yunlin 640, Taiwan, R.O.C.
e-mail: luys@yuntech.edu.tw

1 Introduction

Gear transmissions are usually incorporated in machines that need to provide high torque within a limited space. Among gear transmissions, harmonic drives have the advantages of high gear reduction ratio, compact size, and high torque-to-weight ratio with virtually no backlash. These excellent features make harmonic drives ideal for precise motion mechanisms such as lightweight service robot manipulators [1], force-feedback haptic devices [2] and steer-by-wire systems in the vehicle steering technology [3]. A typical harmonic drive is shown in Fig. 1 [3], which consists of a wave generator, a flexible spline, and a circular spline. The rigid wave generator has an elliptical shape and is enclosed by a flexible race ball bearing. The flexible spline, or "flexspline" for short, is a thin-walled hollow cup, the external gear teeth of which are located at the open end while the closed end of the flexspline is usually connected to an output shaft. The circular spline is a rigid internal gear with two teeth more than the number of teeth on the flexspline. When assembled, the open end of the flexspline becomes elliptic due to the shape of the wave generator, and the flexspline teeth at the major axis of the ellipse engage with the teeth of the circular spline. In the most common configuration, the circular spline is fixed, and a motor drives the wave generator while a load is connected to the flexspline.

In a harmonic drive system, transmission flexibility would cause output oscillations, and frictional forces would deteriorate its output accuracy. To control the output torque of a harmonic drive actuator, Kazerooni [4] employed a sensitivity loop-shaping technique to design a linear controller for the system. Moghaddam and Goldenberg [5] designed a torque controller in an

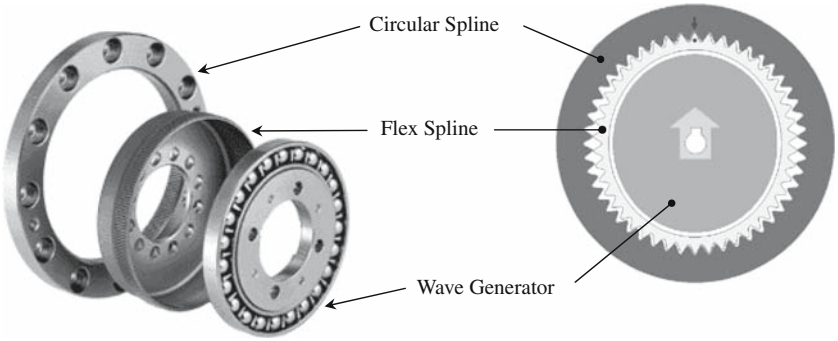

Fig. 1 Constitution of a harmonic drive

H_∞-framework, and Taghirad and Belanger [6] built an H_∞-based torque controller together with a model-based friction compensator. Instead of establishing a friction model that is difficult to be obtained in practice, many researchers [3,7–10] utilized disturbance observers (DOB) [11,12] to estimate unknown torque disturbances. Distinct from high-gain feedback control, the DOB-based compensation estimates the unknown perturbation and generates just the minimum control to regulate plant's dynamics to nominal dynamics. Since the plant's nominal dynamics may not necessarily yield satisfactory performances, the DOB usually accompanies a feedback compensator, such as a PID controller, to shape the nominal dynamics and meet performance requirements. Therefore, in building a DOB-based control system, a feedback compensator as well as a DOB needs to be designed and implemented. Regarding feedback properties, this paper shows the equivalence between the DOB and the so-called Internal Model Control (IMC) [13] that was originally developed for chemical engineering applications. However, the advantage of the IMC scheme is its simple design procedure because the controller parameters are expressed directly in the plant's nominal model and the desired closed-loop dynamics, largely avoiding trial and error. Compared with the DOB-based control configuration, the IMC scheme reduces the efforts required in both the controller design and the practical implementation. Therefore, the IMC is applied to a harmonic drive system as a feedback compensator.

Due to mechanical imperfections such as misalignments of the gear assembly and dimensional inaccuracies of the gear itself, the output torque of the gear contains ripples that vary with different drives, assemblies, and operating conditions. However, a special characteristic of harmonic drives is that the dominating component of ripples is repeated every half turn of the input shaft [14]; that is, the torque ripple is periodic in nature, and its fundamental component corresponds to twice the rotational frequency of the input shaft. To compensate for the kinematic error of a harmonic drive, Nye et al. [15] devised an open-loop method by approximating the kinematic error with a simple sinusoidal term and superimposing it on the desired trajectory. Gandhi and Ghorbel [16] proposed a PD-type controller to compensate for the kinematic error of a harmonic drive in a closed-loop fashion. To reduce speed ripples caused by a harmonic drive, Hirabayashi et al. [17] proposed a method of adaptive speed control, in which the controller senses speed ripples through a high-resolution encoder and modifies the speed command to the driving motor. Godler et al. [18] applied the repetitive control for reducing speed ripples in a harmonic drive system. While the previous studies [15–18] aimed at reducing position or speed ripples, this paper focuses on minimizing torque ripples transmitted to the load.

Adaptive feedforward cancellation (AFC) is an effective method for eliminating a periodic input disturbance, in which the disturbance is simply cancelled by adding the negative of its value at the input of the plant [19]. Since the value of the disturbance is generally unknown, it is adaptively determined by estimating the amplitudes of sine and cosine functions at disturbance frequencies using the output-error signal. The phase difference between the input disturbance and the output error, however, deteriorates the convergence property of the AFC system. Since this phase difference is equal to the phase of the plant at the disturbance frequency, Messner and Bodson [20] and Sacks et al. [21] introduced a phase advance to the basic AFC algorithm in order to compensate for the phase lag due to the plant. To improve the robustness and convergence rate further, Weerasooriya et al. [22] and Zhang et al. [23] used the zero phase error tracking (ZPET) technology [24] to obtain the inverse of the plant's discrete-time model, and fed the output error signal through the plant's inverse model and subsequently to the previous AFC resonator [20,21]. Concerning practical implementations, Lee [25] applied the AFC to the track-following servo for pre-embossed rigid magnet disks while Byl et al. [26] presented the experimental performance of a diamond turning machine with the AFC. The previous AFC schemes [19–23,25,26] extract the periodic disturbance information from the tracking-error signal. Since

the tracking error is directly related to the reference signal, the aperiodic components of the reference would influence the estimation of the periodic disturbance in an adverse way. This paper presents a DOB-based AFC scheme and its application to alleviating torque ripples in a harmonic drive actuator. In the proposed scheme, a DOB is employed in estimating unknown disturbance-cancellation error, and an AFC process suppresses the disturbance components at specific frequencies using the estimated signal of disturbance-cancellation error, rather than using the tracking-error signal in the previous studies. The proposed AFC scheme is then independent of the reference command, and also yields fast convergence of the feedforward cancellation error. Furthermore, the adaptation gain in the proposed AFC process is constrained only by the DOB's dynamics. In other words, with the aid of a DOB, the determination of the AFC's adaptation gain becomes independent of the nominal plant and the feedback compensator. Experiments were conducted on a harmonic dive actuator to show the feasibility and applicability of the proposed scheme.

2 Torque feedback control of a harmonic drive actuator

2.1 Harmonic drive actuator

In the experimental system, the plant to be controlled is a harmonic drive actuator that is a hollow-shaft actuator with an integrated torque sensor, SD-25B from Sensodrive GmbH. Figure 2 shows the schematic diagram of the harmonic drive actuator, which is composed of five major subsystems, namely the torque sensor, harmonic drive gear, eight-pole surface permanent-magnet ac servomotor, power converter and microprocessor. The torque sensor with a Wheatstone bridge of strain gauges is incorporated into the actuator. An instrumentation amplifier is utilized to amplify the differential output voltage of the Wheatstone bridge, yielding a signal indicating the output torque of the harmonic drive actuator. The harmonic drive gear with a gear ratio of $N = 50$ is driven by the ac servomotor equipped with an incremental encoder of 1,500 ppr resolution. Without the brush wear or commutation limit associated with dc servomotors, the ac servomotor is sine-commutated by a fully digital controller. The heart of the digital current controller is the microprocessor that operates the surface permanent-magnet motor with its rotor flux and stator current in quadrature for maximum torque per ampere, i.e. minimum ohmic losses. The developed torque τ_e of the machine is given by $\tau_e = K_t i_q$, where the torque constant $K_t = 30\,(\mathrm{Nm/A})$ referred to the load side and i_q is the quadrature axis current in the d–q synchronously rotating reference frame. In this case, without considering field weakening, the direct axis current i_d in the d–q synchronously rotating reference frame should be zero because it does not contribute to torque production. Here, i_q also represents the peak of the phase current. The overall configuration for controlling the output torque of the harmonic drive actuator has a cascade control structure, which consists of an outer loop which generates the motor torque command to achieve the desired output torque of the harmonic drive actuator, and an inner loop which controls the switching of the inverter so as to have the motor produce the commanded motor torque. That is to say, the control signal $u(t)$ generated by an outer-loop controller is the reference input to the inner loop and represents the desired motor torque referred to the load side. The quadrature axis current command $i_q^*(t)$ to the harmonic drive actuator is thus given by $i_q^*(t) = u(t)/K_t$. In the inner loop, the microprocessor obtains data on the phase currents and desired quadrature axis current through 12-bit A/D converters. It also receives position information from the encoder and generates unit vectors for coordinate transformations. Subsequently, the microprocessor calculates current control laws and produces a sequence of gating signals that are pulse-width modulated (PWM) signals to drive the voltage source inverter whose output is a chopped ac waveform. The cycle time of the current control loops is 0.125 ms, and the PWM switching frequency is correspondingly 8.0 kHz. The rated output power of the actuator is 160 W, and its maximum continuous stall torque is 35 Nm while its maximum output torque reaches 98 Nm.

2.2 Experimental system for the harmonic drive actuator

The experimental system is shown in Fig. 3, in which a floating-point TMS320C6711 digital signal processor (DSP) from Texas Instruments, Inc., is the core of the outer-loop controller, and a Field Programmable Gate Array (FPGA) of model XCV50PQ240-C6 from Xilinx, Inc., processes signals from the shaft encoder to yield a resolution of 6,000 ppr and provides an interface to a 10-bit A/D converter that transforms the analog torque signal into an equivalent digital signal. In real-time control, the DSP obtains the torque and position information from the FPGA, calculates the control algorithms, and sends the control effort to a regulated current converter through a 12-bit D/A converter and some analog signal processing circuits. In the experimental system, a sampling period of 0.1024 ms was chosen, and a personal

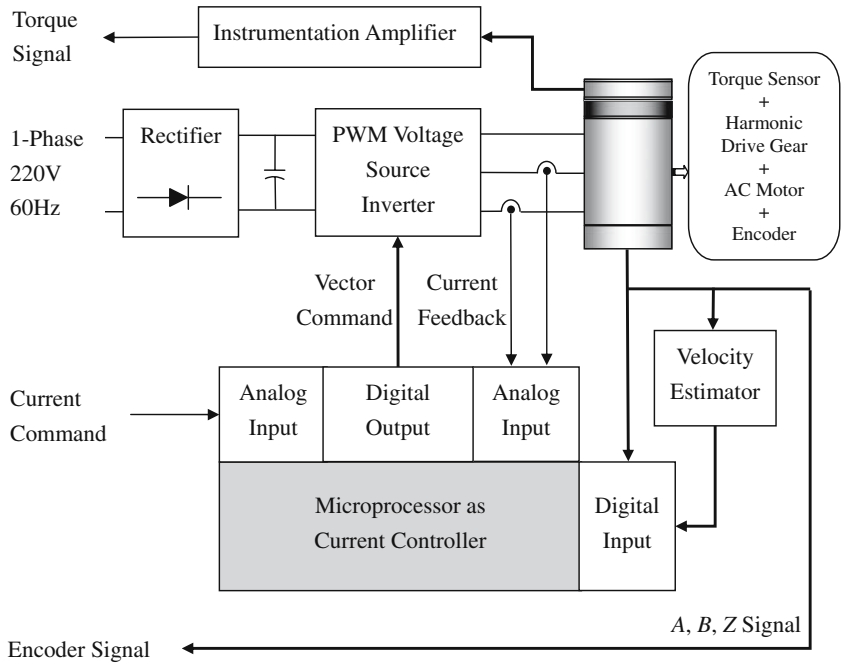

Fig. 2 Configuration of the harmonic drive actuator

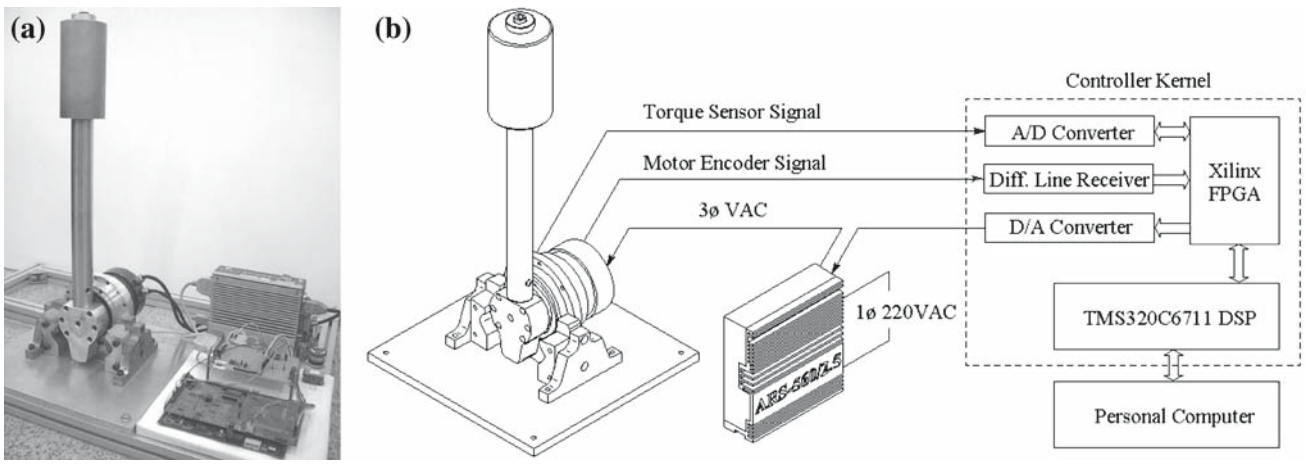

Fig. 3 Experimental system. **a** Photo of the harmonic drive system. **b** Schematic representation of the hardware configuration

computer was used to develop the control program written in C language, to compile it, to download the resulting code into DSP for execution and to acquire experimental data.

In our experimental system, the input to the plant is the motor-torque command to the regulated current converter, and the information on the plant's output is obtained from the torque sensor that measures the output torque of the harmonic drive gear to a load. The identification process is done with the load constrained to the fixed frame. Although there are nonlinearities such as various types of friction and structural damping in the plant, the popular swept-sine approach is used to acquire the frequency response of the plant because of its accuracy even in the presence of extreme noise or nonlinearity, and a linear model is then obtained for the purpose of control. To achieve this, a SigLab 20–42 Dynamic Signal Analyzer (DSA) from Spectral Dynamics, Inc., automatically steps a sine wave over a specified frequency range and measures the frequency response. Subsequently, a Matlab function *invfreqs*$(\cdot)$ performs the least-squares fit to the frequency response data, and yields a nominal transfer function of the plant. Let $P(s)$ denote the transfer function of the plant, $y(s)$ the Laplace transform of the harmonic drive's output torque $y(t)$, and $u(s)$ the Laplace transform of the commanded motor torque $u(t)$ referred to the load side. In this constrained-motion condition, the transfer function

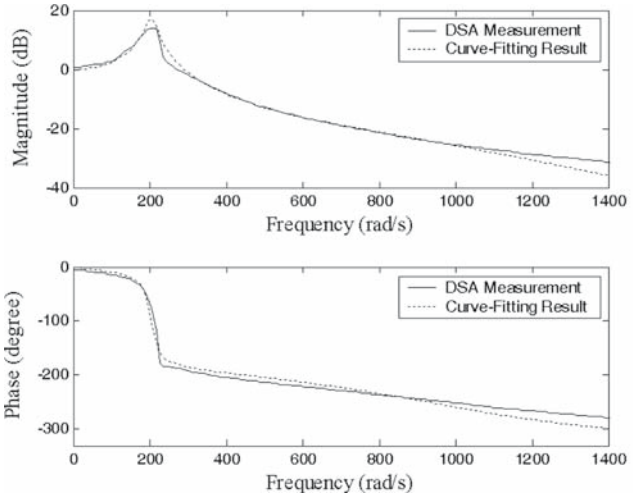

Fig. 4 Measured frequency response and its curve-fitting result

based on the measured frequency response shown in Fig. 4 is

$$P(s) = \frac{y(s)}{u(s)} = \frac{4.83 \times 10^{10}}{s^4 + 998.95s^3 + 1.22 \times 10^6 s^2 + 7.28 \times 10^7 s + 4.84 \times 10^{10}} \quad (1)$$

of which the dc gain is approximately unity as the environment reacts a torque that is equal to the applied one. Moreover, the two pole pairs of the transfer function can be described by $\omega_{n1} = 204.58$ (rad/s), $\zeta_1 = 0.068, \omega_{n2} = 1076.29$ (rad/s), and $\zeta_2 = 0.45$, showing that the structural damping of the harmonic drive actuator is low.

2.3 IMC and its equivalence to DOB

Consider a harmonic drive actuator described by

$$y = P(s)\,(u + d) \quad (2)$$

in which $d(t)$ represents all perturbations referred to the input. As shown in Fig. 5a, the IMC structure uses an internal model $P(s)$ in parallel with the plant $P(s)$. Whenever there is an output difference between the real plant and its model, there is a nonzero feedback to the so-called *IMC controller* $Q(s)P^{-1}(s)$, the feedback controller in the feedforward path of the IMC structure. With the reference r, the output of the IMC system can be derived as

$$y(s) = Q(s)r(s) + (1 - Q(s))\,P(s)d(s) \quad (3)$$

From (3), it is found that, when $Q(s) = 1$, we have $y(s) = r(s)$; that is, the output signal y attains the reference command r instantaneously even in the presence of external perturbations. However, this perfect performance cannot be accomplished in practice since this usually requires control efforts larger than those the actuator can deliver and the *IMC controller* $Q(s)P^{-1}(s)$ is hardly ever proper and cannot be implemented when $Q(s) = 1$. Hence, the filter $Q(s)$ is chosen so that $Q(s)P^{-1}(s)$ is proper, and then its implementation does not involve direct differentiation of the measured output signal with respect to time. When there are no perturbations ($d = 0$), we have $y(s) = Q(s)r(s)$, meaning that the nominal closed-loop transfer function of the IMC system is directly assigned to $Q(s)$. The design of the IMC is hence straightforward, and closed-loop characteristics are related straight to controller parameters [13].

To improve the closed-loop performance of a harmonic drive system, earlier studies [3,7–10] used feedback controllers together with DOBs. Let's manipulate the block diagram of the IMC structure in Fig. 5a by moving $Q(s)P^{-1}(s)$ out of the feedforward path inside the feedback loop as shown in Fig. 5b while leaving the input–output relationship unaffected. Subsequently, rearranging the feedback path in Fig. 5b, we obtain an equivalent block diagram shown in Fig. 5c, where the DOB structure arises. Therefore, the IMC structure is equivalent to the DOB structure together with a feedforward compensator $Q(s)P^{-1}(s)$. It is concluded that the IMC structure possesses the same feedback property as the DOB structure while the IMC approach does not require a feedforward compensator or a nominal controller that is necessary in a DOB-based control system. Therefore, the IMC method is adopted in designing a torque controller for the harmonic drive actuator.

2.4 Shaping dynamic responses with the IMC

For our fourth-order harmonic drive actuator, $Q(s)$ in the IMC structure is denoted as $Q_{\text{im}}(s)$ and is chosen as

$$Q_{\text{im}}(s) = \frac{\omega_{\text{c}}^4}{(s + \omega_{\text{c}})^4} \quad (4)$$

in which ω_{c} is a design parameter to specify desired closed-loop poles. Now, the output response of the closed-loop system can be made fast or slow simply by tuning ω_{c} large or small, respectively. The digital implementation of the IMC involves the discretization of two fourth-order continuous-time models, $Q_{\text{im}}P^{-1}$ and P. In our implementations, the conversion of continuous-time models to discrete-time models is done using the bilinear approximation method with a sampling period of 0.1024 ms. Furthermore, each of the fourth-order discrete-time models is decomposed into two cascaded second-order discrete-time models to reduce the sensitivity to quantization errors in digital implementation

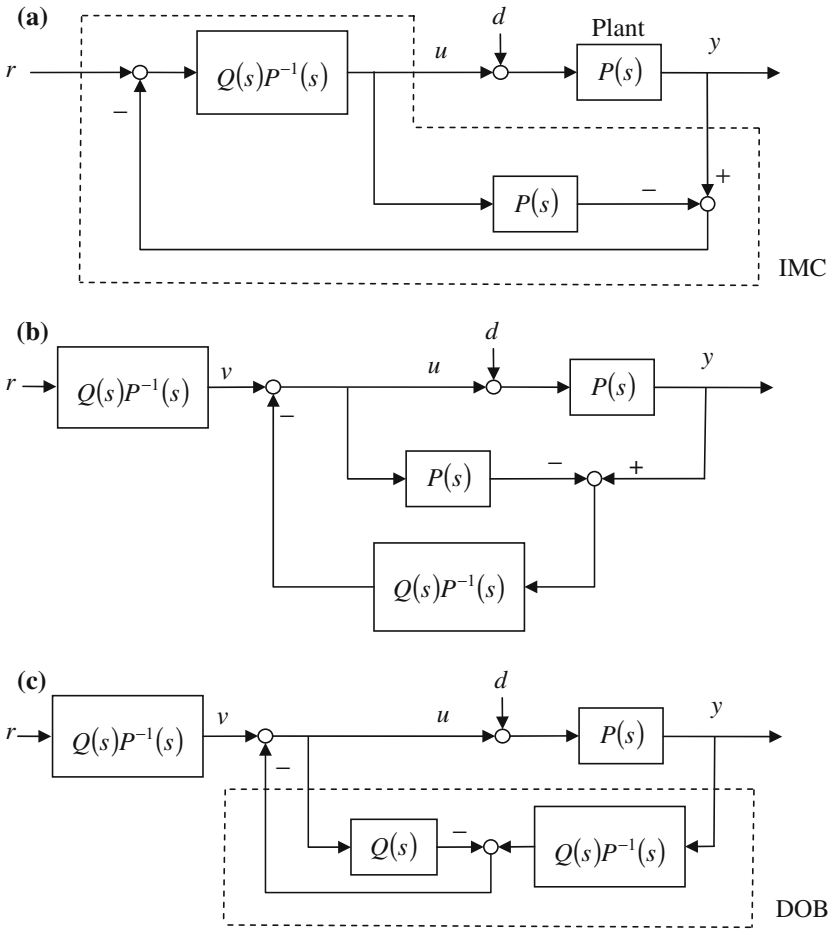

Fig. 5 Alternative representations of the internal model control (IMC) structure and its relation to the disturbance observer (DOB) structure

since a cascade structure results in a smaller range of coefficient values. In order to examine system responses to a stepwise reference command, the load is fixed to the frame such that the actuator is under constrained motion. Figure 6 shows the open-loop and closed-loop responses of the harmonic drive actuator, in which the closed-loop controller has the IMC structure with $\omega_c = 200$ (rad/s). It is seen that the plant itself has low structural damping, and its output torque cannot be controlled well in the open-loop method. Compared with the open-loop control, the IMC improves the output precision, leads to well-damped output responses, and reduces the settling time.

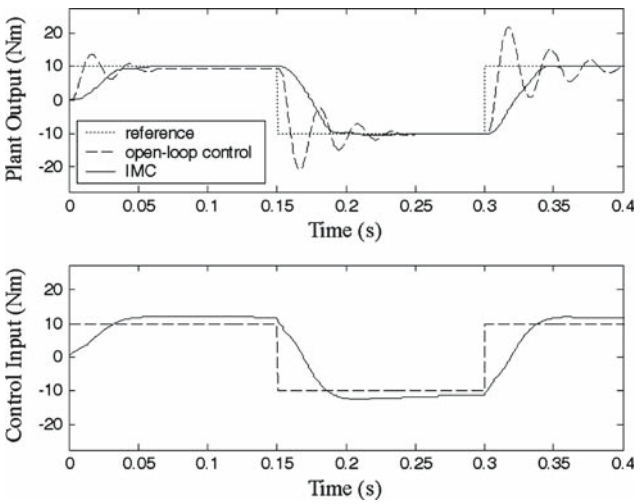

Fig. 6 Dynamical responses of the harmonic drive actuator under constrained motion

3 Alleviation of torque ripples using DOB-based AFC

Harmonic drive gears typically contain kinematic inaccuracies due to manufacturing and assembly errors, leading to output-torque ripples that are periodic with respect to the angular displacement of the input shaft. These torque ripples can be observed in the load motions and even sensed by hand when back-driving the harmonic drive [27]. The main component of these torque ripples occurs twice per wave-generator revolution, for the gear teeth in harmonic drives are meshing in two zones. To measure the transmitted torque,

Hashimoto and Paul [28] firstly proposed the idea of built-in torque sensing, in which Rosette strain gauges are directly mounted on the diaphragm part of the flexspline, an elastic element of a harmonic drive. This method provides an economical way and a compact design of torque sensing for harmonic drives. Some subsequent researches [4–8,27,29–31] continued improving the performance of built-in torque sensing. However, since the flexspline has an elliptical shape, strain gauges directly mounted on the flexspline are subject to unwanted strain that is caused by the elliptical shape [29]. This non-ideal behavior of the sensor practically induces a relatively high signal fluctuation, whose principal frequency is unfortunately also twice the motor speed. This makes it impossible to discern the true ripples caused by gearing meshing vibration from the fluctuation signal caused by non-ideal measurement [27]. Taghirad et al. [27,29] proposed an active compensation of the fluctuation signal by using a Kalman filter with a harmonic oscillator to predict and filter it from the torque measurement. However, since there are actual torque ripples with the same principal frequency as that of the fluctuation signal, this approach also filters the real torque ripples out of the measured torque signal. In our experimental system, the torque signal is obtained from an additional torque sensor with a spring constant higher than that of the flexspline in order to measure the real torque transmitted to the load without reducing the stiffness of the system much. To the best of authors' knowledge, this paper is the first research on compensating for actual torque ripples induced by harmonic drives in the torque control.

3.1 Conventional AFC

Here, the description of the conventional AFC scheme is according to Refs. [21] and [25]. Assume that the unknown disturbance $d(t)$ consists of N sinusoids of known frequencies of the form

$$d(t) = \sum_{i=1}^{N} \{a_i \cos(\omega_i t) + b_i \sin(\omega_i t)\} \tag{5}$$

in which a_i and b_i are unknown, and the subscript i typically refers to the ith harmonic of the fundamental frequency. The AFC design is to construct a control input that exactly cancels the unknown disturbance in (2). Figure 7a shows the conventional AFC structure together with the IMC, in which u_{af} is the disturbance cancellation input by the AFC, u_{fb} denotes the feedback

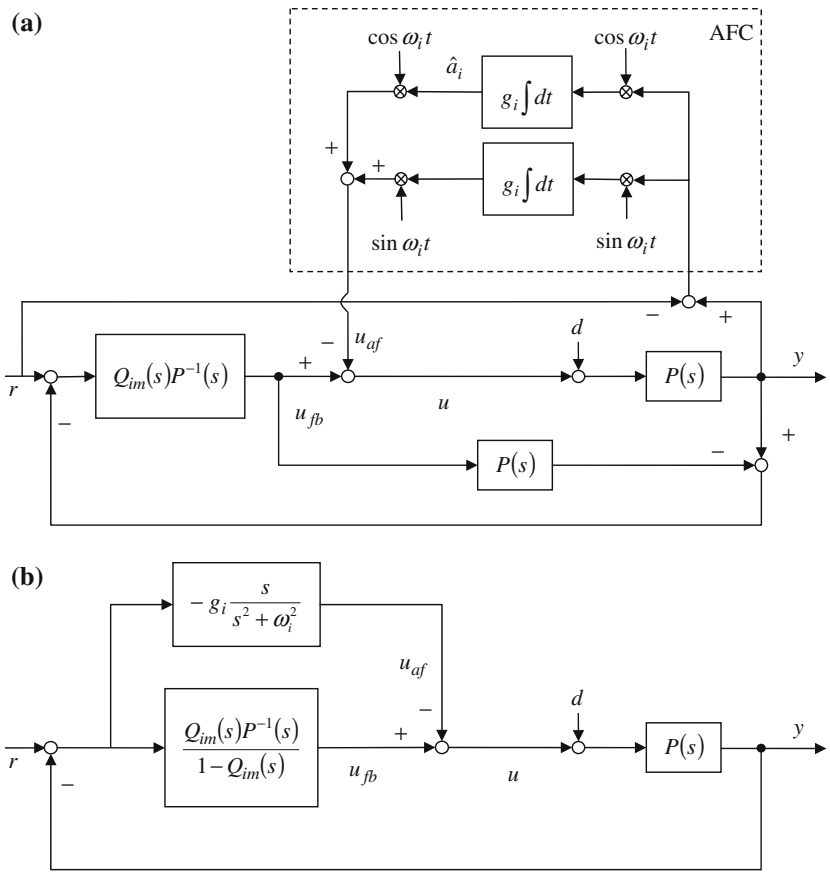

Fig. 7 The conventional AFC scheme. **a** Schematic representation including the IMC. **b** Equivalent block diagram of the conventional AFC system with the IMC

control by the IMC, the control input $u = u_{\rm fb} - u_{\rm af}$, and $\hat{a}_i$ and $\hat{b}_i$ denotes the estimates of a_i and b_i, respectively. The AFC receives the tracking-error signal $(y - r)$, and adjusts $\hat{a}_i$ and $\hat{b}_i$ according to the following adaptation laws:

$$\hat{a}_i = g_i \int (y - r)\cos(\omega_i t)\mathrm{d}t \tag{6}$$

$$\hat{b}_i = g_i \int (y - r)\sin(\omega_i t)\mathrm{d}t \tag{7}$$

in which parameter g_i is a constant adaptation gain. Subsequently, the AFC determines the feedforward control as

$$u_{\rm af} = \sum_{i=1}^{N} \left\{ \hat{a}_i \cos(\omega_i t) + \hat{b}_i \sin(\omega_i t) \right\} \tag{8}$$

in order to reject the input disturbance $d(t)$. Based on a Laplace transform analysis of the AFC structure [19], there is an equivalent linear time-invariant (LTI) representation as follows:

$$C(s) = \sum_{i=1}^{N} g_i \frac{s}{s^2 + \omega_i^2} \tag{9}$$

which is the transfer function from $(y - r)$ to $u_{\rm af}$. With this model of the AFC resonator, a block diagram of the AFC system is shown in Fig. 7b, in which the IMC structure is equivalently represented by the classic unit-feedback structure with a compensator $Q_{\rm im}(s)P^{-1}(s)/(1 - Q_{\rm im}(s))$. The LTI analysis can then be applied for analyzing its stability. Particularly, an upper bound on the adaptation gain g_i can be determined using a Nyquist plot or a root locus. From Fig. 7b, it is seen that the range of the adaptation gain for a stable AFC system depends on the plant and the compensator as well. There are three drawbacks of the conventional AFC structure. Firstly, the adaptation gain needs to be redesigned whenever there is a change in the plant or the feedback compensator. Secondly, since the upper bound on the adaptation gain is constrained by both the plant and the compensator, it would yield a small adaptation gain and thus slow convergence. Thirdly, due to the use of the tracking error as the input to the AFC resonator, aperiodic variations in the reference command would affect the adaptive dither and bring forth unsatisfactory transient responses.

3.2 DOB-based AFC

The previous AFC schemes [19–23,25,26] update the disturbance-cancellation control according to output errors, extracting disturbance information from output errors indirectly. As shown in Fig. 8a, the proposed

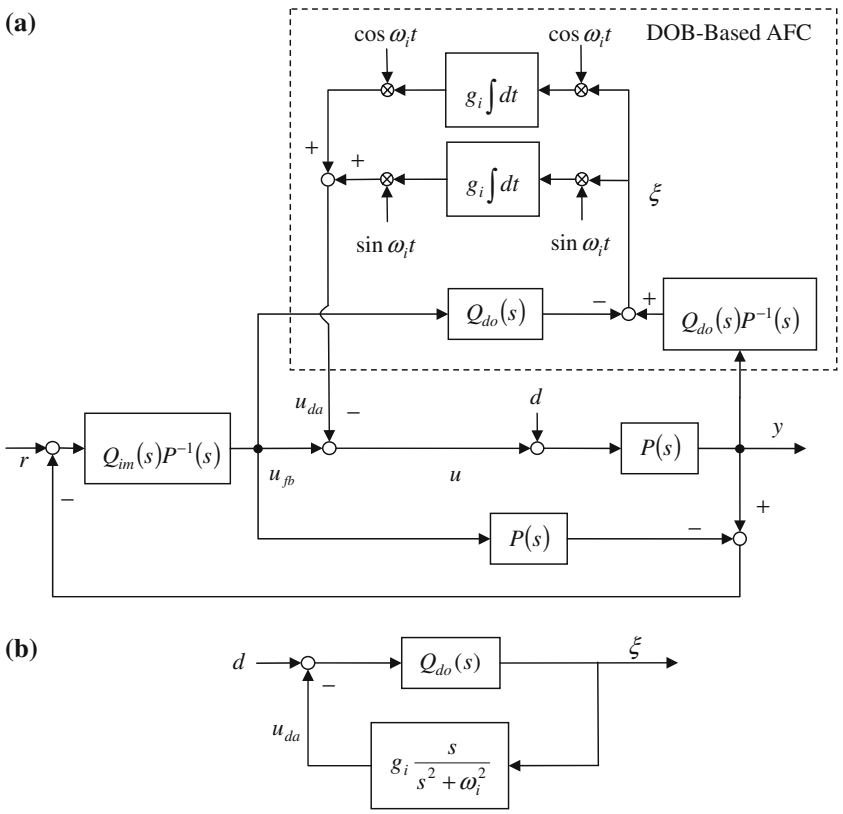

Fig. 8 The proposed DOB-based AFC scheme. **a** Schematic representation including the IMC. **b** Equivalent block diagram of the proposed AFC loop

DOB-based AFC scheme consists of a DOB and an AFC resonator. The DOB evaluates the difference between the unknown disturbance and the cancellation control, and the AFC block adapts the disturbance-cancellation control u_{da} according to the DOB's estimate of disturbance-cancellation error, rather than the output tracking error. In a DOB, the filter $Q_{\mathrm{do}}(s)$ is chosen so that $Q_{\mathrm{do}}(s)P^{-1}(s)$ is proper, and then its implementation does not involve direct differentiation of the measured output signal with respect to time. The DOB's output $\xi(t)$ can be derived as

$$\xi(s) = Q_{\mathrm{do}}(s)\left(-u_{\mathrm{da}}(s) + d(s)\right) \tag{10}$$

Utilizing the DOB's output, the proposed AFC adjusts $\hat{a}_i$ and $\hat{b}_i$ according to the following adaptation laws:

$$\hat{a}_i = g_i \int \xi(t)\cos(\omega_i t)\mathrm{d}t \tag{11}$$

$$\hat{b}_i = g_i \int \xi(t)\sin(\omega_i t)\mathrm{d}t \tag{12}$$

Subsequently, the adaptive feedforward control is determined as

$$u_{\mathrm{da}} = \sum_{i=1}^{N}\left\{\hat{a}_i\cos(\omega_i t) + \hat{b}_i\sin(\omega_i t)\right\} \tag{13}$$

According to (10), the DOB's output is decoupled from the IMC feedback loop, and the stability of the AFC loop is thus independent of the feedback compensator. Figure 8b shows an equivalent block diagram of the proposed AFC loop, and its stability depends solely on the AFC resonator and the filter $Q_{\mathrm{do}}(s)$ that represents the DOB's dynamics. Therefore, the proposed AFC structure simplifies the stability analysis when compared with the conventional AFC structure, and the adaptation gains can be identical for various applications by keeping the DOB's dynamics unchanged. The improvements of the proposed AFC scheme over the conventional one are: (1) the redesign of the adaptation gain is not required when there is a change in the nominal model or the feedback compensator; (2) the proposed AFC directly uses the estimated disturbance-cancellation error to adjust the disturbance-cancellation control, yielding fast convergence of the cancellation error; and (3) the disturbance-cancellation process is not influenced by aperiodic variations in the reference command.

3.3 Torque-ripple compensation with the AFCs

The conventional AFC and the proposed AFC are applied to compensating for the major torque ripple whose frequency is twice the angular frequency of the input shaft. Since the torque ripples induced by harmonic drives are periodic functions of position instead of time, the time in the AFC's formulation is implemented with the angular position, and the sine and cosine functions in the AFC block are modified to $\sin(2\theta_m)$ and $\cos(2\theta_m)$, respectively, in which θ_m denotes the angular position of the motor shaft that is fixed to the wave generator. To verify the effectiveness of the proposed scheme, consider the harmonic drive actuator in free motions under two kinds of operating conditions: quasi-constant angular-speed motion and variable angular-speed motion.

In quasi-constant angular-speed motion, the servomotor is forced to have an initial speed of approximately 11.4 (rps) at the beginning of a torque-control task, and the output torque of the harmonic drive actuator

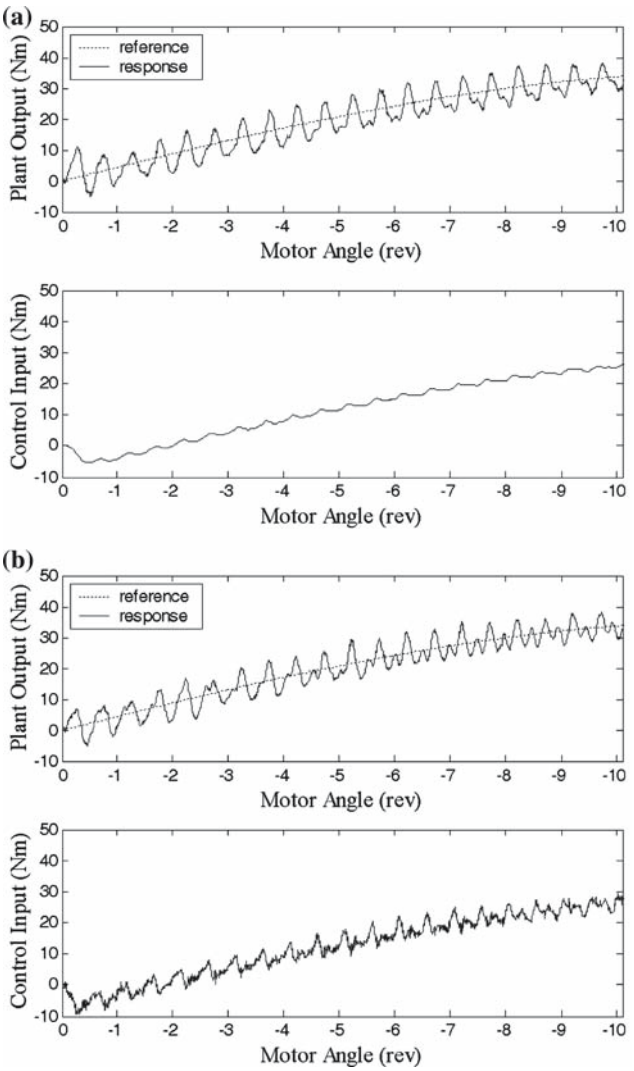

Fig. 9 Tracking responses of the IMC under quasi-constant speed motion with various closed-loop bandwidths. **a** With $\omega_c = 200$ (rad/s). **b** With $\omega_c = 600$ (rad/s)

is then required to counteract the effect of the gravitational force exerted on the load, that is, the torque reference $r = -35.4 \sin(\theta_m/N)$ (Nm) in our setup. When the output torque perfectly follows the reference, the load will move at a constant velocity as if it was in the outer space and without external forces. Figure 9 shows the tracking performance of the IMC without AFC, in which various values of the closed-loop bandwidth are examined by tuning the parameter ω_c in the IMC structure. It can be seen that the high-gain feedback control by increasing the closed-loop bandwidth is not an effective approach to compensating for torque ripples since the effects of sensor noise on the control become significant and torque ripples are not minimized well. Figure 10 shows the tracking responses of the conventional AFC with $g_2 = 3.5$ and $g_2 = 6.5$, in which

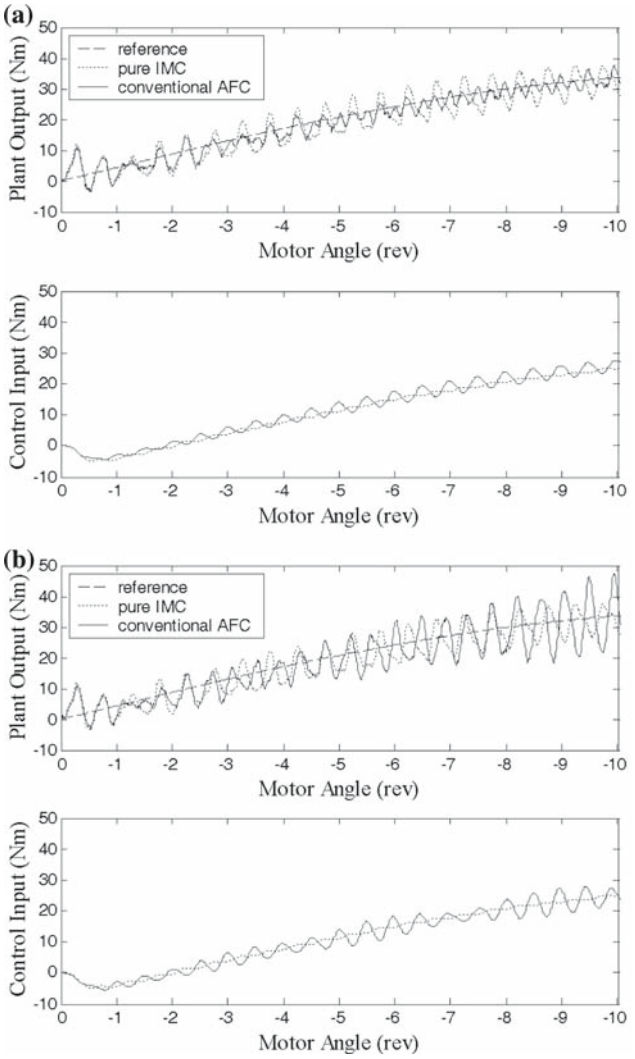

Fig. 10 Tracking responses of the conventional AFC under quasi-constant speed motion with different adaptation gains. **a** With $g_2 = 3.5$. **b** With $g_2 = 6.5$

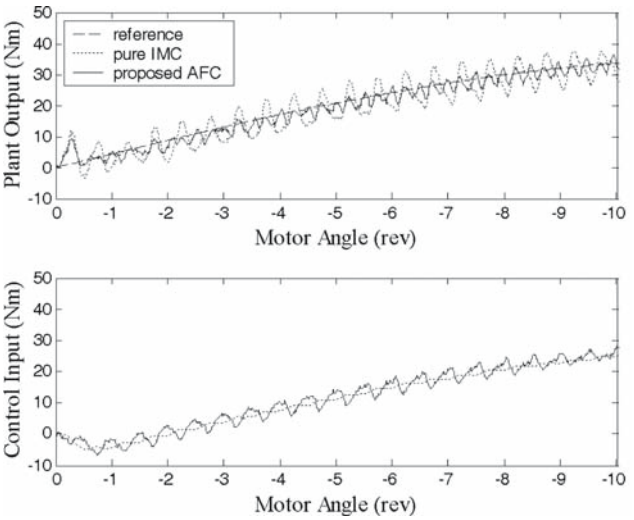

Fig. 11 Tracking responses of the proposed AFC under quasi-constant speed motion

the AFC control with $g_2 = 3.5$ takes approximately three motor revolutions to become effective in canceling the main disturbance. The large adaptation gain $g_2 = 6.5$ reduces the required transient interval to about one motor revolution, but the output response diverges gradually. Figure 11 shows the dynamic response of the proposed AFC with $g_2 = 100$, in which $Q_{do}(s)$ is designed as a fourth-order low-pass Butterworth filter with a cut-off frequency of 180 Hz. It is seen that the proposed AFC becomes effective soon after half a motor revolution, showing that the proposed scheme improves the convergence speed and robustness of the conventional AFC.

A torque-controlled actuator does not necessarily operate at a constant speed. To evaluate the performance of the proposed control scheme in variable angular-speed motion, we apply the following reference:

$$r = \begin{cases} -35.4 \sin(\theta_m/N) - 1.2 \text{ (Nm)} & \text{for } |\theta_m| \leqslant 10\pi \text{ (rad)}, \\ -35.4 \sin(\theta_m/N) + 1.2 \text{ (Nm)} & \text{for } |\theta_m| > 10\pi \text{ (rad)} \end{cases} \tag{14}$$

which, when followed precisely, accelerates the load during the first five revolutions of the motor shaft, and decelerates the load afterwards. Figure 12 shows the tracking performance of the proposed AFC. From the output response of the IMC without AFC, it is seen that the magnitude of torque ripples varies with the angular speed of the input shaft. From Fig. 12a, it is obvious that the tracking performance of the pure IMC has been improved by the proposed AFC even when the amplitude of torque ripples is time-varying. However, it is seen from Figs. 11 and 12a that there exist leftover torque ripples which mainly contain the fourth-harmonic component. Since the sinusoidal permanent-magnet ac machine

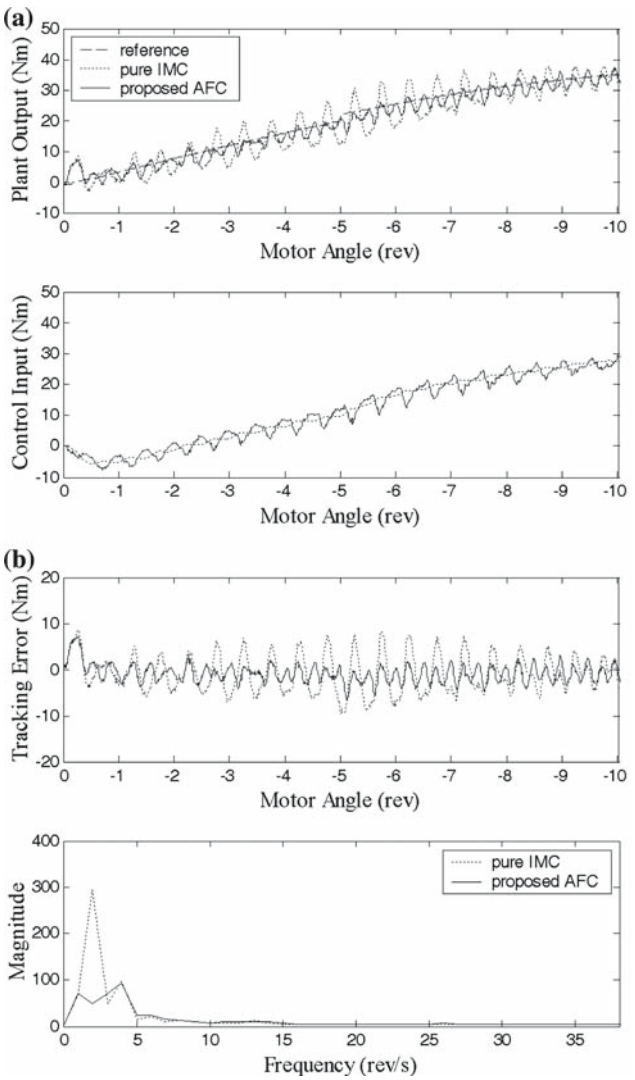

Fig. 12 Performance of the proposed AFC under variable speed motion. **a** Dynamic responses. **b** Tracking errors and their spectra

has four pole pairs, this remaining component is likely to be ascribed to the current offsets or different pole flux levels of the four pole pairs, possibly combined with rotor eccentricity. Figure 12b shows the spectra of the tracking error, demonstrating that the torque ripples of twice the frequency of the motor shaft is alleviated while keeping other frequency components almost unaltered.

4 Conclusions

Regarding feedback properties, this paper demonstrates that the IMC structure is equivalent to the DOB structure. However, for command tracking, the IMC structure possesses the advantage of ease in design and implementation over the DOB-based control configuration. The IMC is thus employed in shaping the dynamics of a harmonic drive actuator. On the other hand, the DOB directly reveals the information on input disturbances, and is applied to improve the conventional AFC scheme. The proposed DOB-based AFC brings about three benefits. Firstly, the stability of the proposed AFC system is independent of the plant and the feedback compensator, and thus the adaptation gain needs no redesign after readjusting the plant or retuning the feedback compensator. Secondly, with the aid of the DOB, the proposed scheme yields a convergence rate faster than that of the conventional AFC scheme which indirectly extracts the disturbance information from the tracking error. Thirdly, aperiodic changes in the reference command do not induce undesirable transient responses of the AFC resonator. The experimental results show that the proposed scheme comprising the IMC and the DOB-based AFC not only improves the dynamics of a harmonic drive actuator, but also adaptively and effectively alleviates the major component of torque ripples induced by the harmonic drive.

Acknowledgments The authors would like to thank the Institute of Robotics and Mechatronics, German Aerospace Center for the use of its facilities. The supports from N. Sporer, M. Haehnle and M. Hauschild are also gratefully acknowledged. This work was partially supported by the National Science Council of ROC under grant number NSC 93-2218-E-224-004.

References

1. Hirzinger G, Sporer N, Schedl M, Butterfaß J, Grebenstein M (2004) Torque-controlled lightweight arms and articulated hands: do we reach technological limits now? Int J Rob Res 23(4):331–340
2. Ueberle M, Buss M (2002) Design, control, and evaluation of a new 6 DOF haptic device. In: Proceedings of IEEE International Conference Intelligent Robot Systems, Lausanne, Switzerland, pp 2–4
3. Bajcinca N, Hauschild M, Cortesao R (2003) Robust torque control of steer-by-wire vehicles. In: Proceedings of International Conference Advanced Robot, Portugal, pp 1480–1486
4. Kazerooni H (1995) Dynamics and control of instrumented harmonic drives. J Dyn Syst Meas Control Trans ASME 117(1):15–19
5. Moghaddam MM, Goldenberg AA (1997) On robust control of flexible joint robots using describing function and sector bounded nonlinearity descriptions. J Intell Robot Syst 20: 333–348
6. Taghirad HD, Belanger PR (2001) H_∞-based robust torque control of harmonic drive systems. J Dyn Syst Meas Control Trans ASME 123:338–345
7. Godler I, Hashimoto M (1998) Torque control of harmonic drive gears with built-in sensing. In: Proceedings of IECON, Aachen, Germany, pp 1818–1823

8. Hashimoto M, Kiyosawa Y (1998) Experimental study on torque control using harmonic drive built-in torque sensors. J Robotic Syst 15(8):435–445
9. Kaneko K, Murakami T, Ohnishi K, Komoriya K (1994) Torque control with nonlinear compensation for harmonic drive dc motors. In: Proceedings of IECON, Bologna, Italy, pp 1022–1027
10. Sato K, Zheng J, Tanaka T, Shimokohbe A (2000) Micro/macro dynamic characteristics of mechanism with a harmonic speed reducer and precision rotational positioning control using disturbance observer. JSME Int J Ser C 43(2):318–325
11. Komada S, Ishida M, Ohnishi K, Hori T (1991) Disturbance observer-based motion control of direct drive motors. IEEE Trans Energy Convers 6(3):553–559
12. Umeno T, Hori Y (1991) Robust speed control of dc servomotors using modern two degrees-of-freedom controller design. IEEE Trans Ind Electron 38(5):363–368
13. Morari M, Zafiriou E (1989) Robust process control. Prentice-Hall, Englewood Cliffs, NJ
14. Hidaka T, Zhang Y, Sasahara M, Tanioka Y (1989) Vibration of a strain wave gearing in an industrial robot. In: Proceedings of ASME International Power Transmission and Gearing Conference, pp 789–794
15. Nye T, Kraml R (1991) Harmonic drive gear error: characterization and compensation for precision pointing and tracking. In: Proceedings Aerospace Mechanics Symposium, California, USA, pp 237–252
16. Gandhi FS, Ghorbel F (2002) Closed-loop compensation of kinematic error in harmonic drives for precision control applications. IEEE Trans Contr Syst T 10(6):759–768
17. Hirabayashi H, Chiba J, Akahane A (1990) Vibration suppression of strain wave gearing. In: Proceedings of JSME Conf Robotics and Mechatronics, Japan, pp 789–794
18. Godler I, Ohnishi K, Yamashita T (1994) Repetitive control to reduce speed ripple caused by strain wave gearing. In: Proceedings of IECON, Bologna, Italy, pp 1034–1038
19. Bodson M, Sacks A, Khosla P (1994) Harmonic generation in adaptive feedforward cancellation scheme. IEEE Trans Autom Control 39(9):1939–1944
20. Messner W, Bodson M (1994) Design of adaptive feedforward controllers using internal model equivalence. In: Proceedings of American Control Conference, Maryland, pp 1619–1623
21. Sacks A, Bodson M, Messner W (1995) Advanced methods for repeatable runout compensation. IEEE Trans Magn 31(2):1031–1036
22. Weerasooriya S, Zhang JL, Low TS (1996) Efficient implementation of adaptive feedforward cancellation in a disk drive. IEEE Trans Magn 32(5):3920–3922
23. Zhang JL, Chen R, Guo G, Low TS (2000) Modified adaptive feedforward runout compensation for dual-stage servo system. IEEE Trans Magn 36(5):3581–3584
24. Tomizuka M (1987) Zero phase error tracking algorithm for digital control. J Dyn Syst Meas Control Trans ASME 109: 65–68
25. Lee HS (1997) Implementation of adaptive feedforward cancellation algorithms for pre-embossed rigid magnetic (PERM) disks. IEEE Trans Magn 33(3):2419–2423
26. Byl MF, Ludwick SJ, Trumper DL (2000) A loop shaping perspective for tuning controllers with adaptive feedforward cancellation. Precis Eng 29:27–40
27. Taghirad HD, Belanger PR (1999) Intelligent built-in torque sensor for harmonic drive systems. IEEE Trans Instrum Meas 48(6):1201–1207
28. Hashimoto M, Paul RP (1987) Integration of manipulator joint sensor information for robust robot control. In: Proceedings of IEEE Conference Decisan Control, pp 603–604
29. Taghirad HD, Belanger PR (1998) Torque ripple and misalignment torque compensation for the built-in torque sensor of harmonic drive systems. IEEE Trans Instrum Meas 47(1):309–315
30. Godler I, Horiuchi M, Hashimoto M, Ninomiya T (2000) Accuracy improvement of built-in torque sensing for harmonic drives. IEEE/ASME Trans Mech 5(4):360–366
31. Godler I, Hashimoto M, Horiuchi M, Ninomiya T (2001) Performance of gain-tuned harmonic drive torque sensor under load and speed conditions. IEEE/ASME Trans Mech 6(2):155–160